Modelling the emergence of spiral colony morphology in the yeast *Magnusiomyces magnusii*

Kai Li[1] Andrew J. Black[2] Tea Knežević[3] Jennifer M. Gardner[4] Jin Zhang[5] Vladimir Jiranek[6] J. Edward F. Green[7] Benjamin J. Binder[8] Alexander K. Y. Tam[9]

September 15, 2025

Abstract

Yeast species have several adaptations that enable them to survive in harsh environments. These adaptations can include biofilm formation, where the secretion of extracellular polymeric substances can protect the cells from a hostile environment, or, under nutrient-limited conditions, pseudohyphal or hyphal growth, where the colony can send out long 'tendrils' to explore the environment and seek nutrients. Recently, we observed a spiral colony morphology emerge in an isolate of the hyphae-forming yeast *Magnusiomyces magnusii* grown under laboratory conditions. We use an off-lattice agent-based model (ABM) that simulates colony development to investigate the hypothesis that

the spiral morphology is the result of bias in the hyphal branching angle. The model involves biologically-motivated rules of hyphal growth and branching, with key model parameters including the colony size at the onset of hyphal filaments, and the branching angle. Using one example of an experimentally-grown colony, we use a sequential neural likelihood method to perform likelihood-free Bayesian inference to infer the model parameters. Our results indicate a mean hyphal branching angle of 2.3° [1.1°, 3.6°] (95% credible interval). To confirm the model's applicability to colony growth, we use biologically-feasible parameter values to yield a range of morphologies observed in *M. magnusii* experiments.

1 Introduction and background

Yeasts are unicellular eukaryotic organisms that have diverse impacts on human life. A major negative impact is their ability to colonise implanted medical devices such as catheters, prostheses, and stents [33, 39]. Yeasts such as *Candida albicans* and *Candida auris* are opportunistic pathogens responsible for up to 44% of severe hospital-acquired infections [56], which have mortality rates of between 15–35% [50, 2]. Yeasts are infectious because they can invade surrounding tissue [19], thanks, at least in part, to their ability to form hyphae [11] or pseudohyphae [27, 8]. Therefore, some scientific work on yeasts has focused on understanding cellular behaviours that give rise to macroscopic patterns in pseudohyphal [36] or hyphal [40, 41] colonies. Much of this work involves the species *Saccharomyces cerevisiae*, which was the first eukaryotic organism to have its genome fully sequenced [28]. Since

then, this yeast has become an even more common model organism in cell biology research [10, 12], aiding understanding of pathogenic yeasts [7], and the behaviour of eukaryotic cells more generally [12].

S. cerevisiae also has uses in the production of food (as reflected by its common name of 'baker's yeast'), medicines [1], and biofuels [38]. Another common use of yeast is in brewing alcoholic beverages, where optimisation of yeast strains is an ongoing area of innovation in wine production [25, 61]. Strain optimisation increasingly involves bioprospecting, the process of uncovering new strains in natural habitats, as winemakers seek improved quality and fermentation efficiency [31]. This continual discovery of new strains motivates ongoing scientific research into understanding differences in growth between yeast species and strains in different experimental conditions.

The range of yeasts' impact on life is mirrored by their diversity in modes of growth. Many different modes can be reproduced in laboratory experiments, as illustrated in Figure 1. These morphologies are mediated by factors including the yeast species, genetic make up [55], adhesins [69], nutrient availability [67, 64, 58, 27], quorum sensing [30, 46] and the mechanical properties of the medium on which they are grown [51, 53]. On soft substrates, yeasts can form colony biofilms that can grow over a 90 mm Petri dish in 1–2 weeks [4, 6, 54, 55, 58]. This form of growth is illustrated in Figures 1a–1d. The distributions of viable and dead cells within these colonies can vary spatially [52, 66], and understanding the roles of cell death in yeast colonies is an important subject of research [15, 47, 29, 65]. Yeasts can enter a stationary phase that enables them to survive [43] harsh environments. In seemingly opposite behaviour, yeasts can also undergo regulated cell death [16], an altruistic

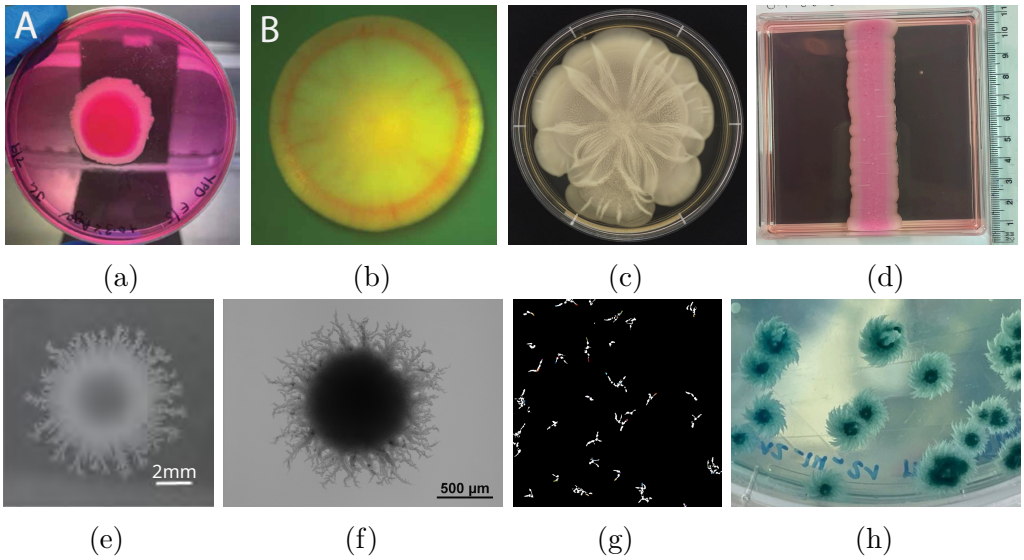

Figure 1: Comparison of yeast colony patterns in different experimental environments. (a) *M. magnusii* colony biofilm after seven days of growth. Dark regions indicate elevated cell death occurring in a central region resembling a necrotic core, which probably occurs due to accidental cell death (ACD) [45]. (b) *S. cerevisiae* colony biofilm after five days of growth. The red ring indicates elevated cell death, which is probably due to regulated cell death (RCD) [45]. (c) *S. cerevisiae* colony biofilm grown on nutrient-rich soft (0.3%) agar [54, 55, 58]. (d) Rectangular *S. cerevisiae* colony biofilm on (0.6%) YPD media. Darker regions indicate elevated cell death compared to lighter regions [59] (e) *S. cerevisiae* colony grown on YND after 58 days of growth [63]. (f) Filamentous yeast of the *S. cerevisiae* strain AWRI 796, with 50 µM nutrients [8]. (g) Early stages of hyphal colony formation in *Candida albicans* [37] (h) Hyphal *M. magnusii* colonies grown on a Petri dish with high colony density.

process that releases nutrients for future consumption [45]. One method for characterising cell death with colonies is to stain them with Phloxine B [42] dye. As illustrated in Figures 1a and 1b, this staining creates darker pink regions indicating elevated cell death. In Figure 1a, cell death occurs near the centre of the colony. This death is likely to be accidental cell death due to lack of nutrients, similar to a necrotic core. Conversely, in Figure 1b cell death is localised in a ring trailing the leading edge. This death may be due to regulated cell death [45], which releases nutrients near the leading edge to promote further proliferation. These different forms of cell death highlight yeast's diversity of growth.

Colony biofilm growth is also influenced by nutrient availability [58, 67]. In low-nutrient environments, yeasts form very different morphologies to colony biofilms by producing smaller colonies with non-uniform spatial structure (Figures 1e and 1f). Interestingly, Tronnolone et al. [64] found that yeasts, which are non-motile, also cannot respond actively to nutrient gradients. This provided evidence that the non-uniform patterns in Figures 1e and 1f form due to pseudohyphal growth [27, 8, 63], rather than directed growth in response to environmental gradients. Pseudohyphal growth involves a switch between unipolar and bipolar budding and the creation of elongated chains of unipolar cells [27], allowing the colony to extend radially to obtain nutrients, and to invade agar surfaces. Similar to moulds, yeasts can also form hyphal colonies, where the yeast grows in elongated tubes consisting of multiple cells. Figure 1g depicts the early stages of hyphal colony development. Hyphal growth is also affected by many factors, for example carbon dioxide levels [49]. These different colony morphologies illustrate that diversity of outcome is a key

characteristic of yeast growth. Given that new strains are being continuously discovered by bioprospecting, there is an incentive for developing robust mathematical modelling and parameter inference methods to understand these new strains. We outline such a procedure in this manuscript.

In search of improved wine strains, we bioprospected a new isolate of *M. magnusii* from the sap of a Tasmanian cider gum tree, *Eucalyptus gunnii*. Under laboratory conditions, this yeast formed a novel highly ordered spiral morphology (Figure 1h). This spiralling morphology does not appear on all growth media (data not shown) and thereby appears to represent another adaptation that a yeast has developed in response to environmental cues. Like *S. cerevisiae*, *M. magnusii* colonies create filaments that extend radially from a circular Eden-like [23] region. Unlike *S. cerevisiae*, where the filaments consist of elongated yeast cells, the main branch of the *M. magnusii* filament consists of stiff rod-like hyphae [21] that are 7–12 µm wide. Penicillate secondary branches emerge at acute angles from the main branch, forming a bushy or fan-like arrangement. These thinner secondary branches break apart into arthroconidia, which are rectangular spore-like units 4–7 µm wide and 10–18 µm long (Figure 2). Non-uniform spatial patterns also emerge in hyphal *C. albicans* colonies [7, 18, 44], but they do not exhibit the striking spiral patterns of *M. magnusii*. The cell-scale mechanisms that underpin these spiral colonies of *M. magnusii* remain to be determined.

Depending on the type of growth considered, mathematical models of yeast colonies have involved agent-based [36, 5], reaction–diffusion [17, 58, 34], and continuum mechanical [57, 60] approaches. Owing to the small size of individual *M. magnusii* colonies, we use an off-lattice agent-based model [63,

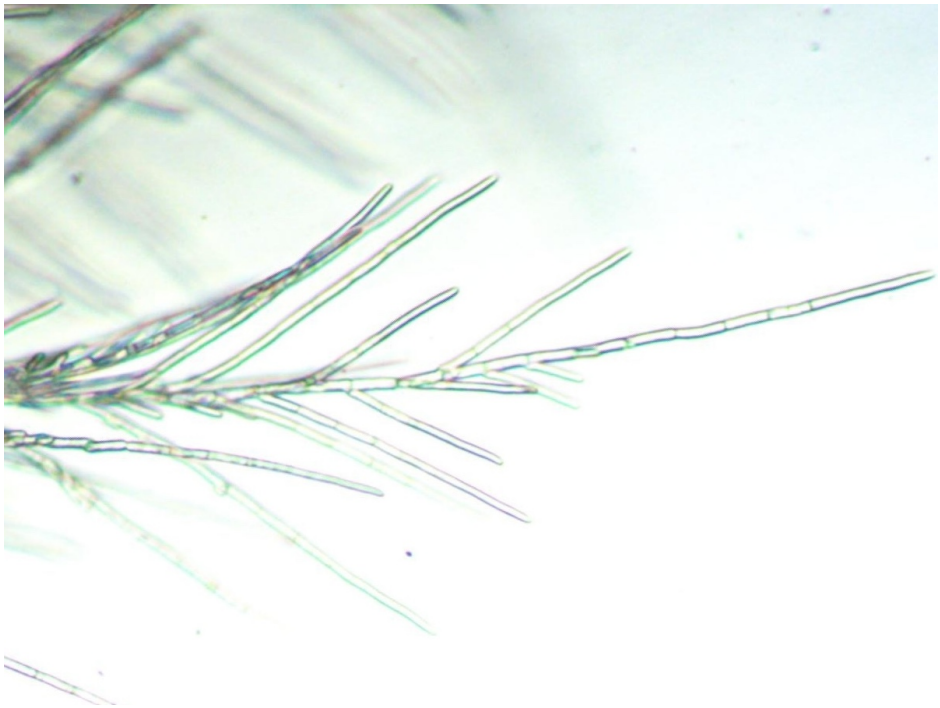

Figure 2: Branching pattern of a hyphal *M. magnusii* colony.

24, 13, 32, 14, 68] to simulate the spiral morphology. Our objective is to understand how cellular behaviour gives rise to colony-scale patterns. Agents in the model represent rod-like segments of fixed size. These segments could represent hyphae, segments of a rod-like hyphal filaments, or arthroconidia in a secondary branch. In the model, regular hyphae and arthroconidia can extend from sites located on the sides of the cell, whereas rod-like hyphae extend end-to-end only, with a prescribed angle between segments. To compare the model with the experiment, we use image processing and Bayesian inference using neural likelihood estimation [48, 3, 22]. The shape of the hyphal colony components is mainly governed by the hyphal branching angle. Using realistic parameter estimates, the model can also capture three other distinct colony morphologies formed by *M. magnusii* grown under different conditions.

2 Yeast growth experiments

An in-house isolate of *Magnusiomyces magnusii* was used for these experiments. Yeast was cultured in liquid Yeast Peptone Dextrose medium (YPD; $10\,\mathrm{g\,L^{-1}}$ yeast extract, $20\,\mathrm{g\,L^{-1}}$ peptone, $20\,\mathrm{g\,L^{-1}}$ glucose) with 2% agar where solid medium was required. 5 mL yeast cultures were grown for 48 hours in liquid YPD prior to inoculation onto 90 mm round agar plates where a 50 µL aliquot diluted to $4 \times 10^2\,\mathrm{cells\,mL^{-1}}$ (low cell density) or $4 \times 10^3\,\mathrm{cells\,mL^{-1}}$ (high cell density) with Phosphate Buffered Saline was spread plated. Agar plates contained either Chemically Defined Sap Medium (CDS; $10\,\mathrm{g\,L^{-1}}$ yeast extract, $20\,\mathrm{g\,L^{-1}}$ peptone, $15\,\mathrm{g\,L^{-1}}$ glucose, $12\,\mathrm{g\,L^{-1}}$ fructose, $9\,\mathrm{g\,L^{-1}}$ maltose, $2\,\mathrm{g\,L^{-1}}$ glycerol, 1% (v/v) ethanol, $1\,\mathrm{g\,L^{-1}}$ acetic acid, $1\,\mathrm{g\,L^{-1}}$ pyruvic acid, $2\,\mathrm{g\,L^{-1}}$ gluconic acid, $0.1\,\mathrm{g\,L^{-1}}$ succinic acid) or Yeast Nitrogen Base (YNB; Becton Dickinson; Cat No. 233520), prepared according to the manufacturer's instructions and with the addition of $2\,\mathrm{g\,L^{-1}}$ D-glucose and $5\,\mathrm{g\,L^{-1}}$ ammonium sulfate. Plates were sealed with Parafilm and incubated at 25 °C for 5-10 days. Macroscopic plate images were captured with an Apple iPhone 12 Pro and microscopic imaging with a Leica M-Z FL111 microscope with a Nikon DS-5MC Microscope Camera and Nikon NIS element software or a Carl Zeiss Axiophot Pol Photomicroscope with a Toupcam UCMOS Microscope Camera and ToupView software.

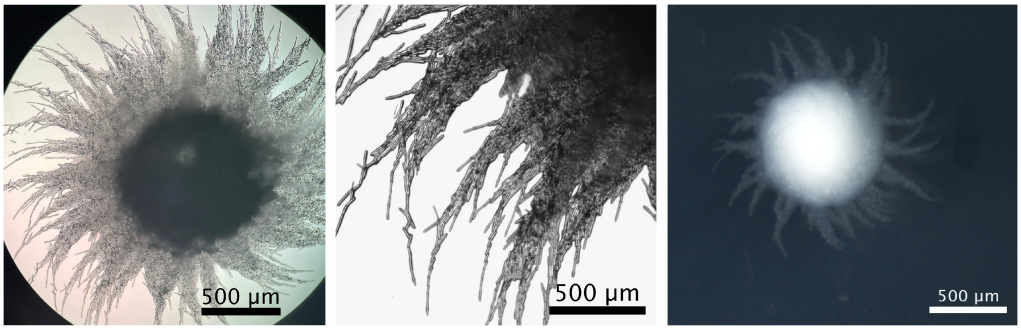

(a) (b) (c)

Figure 3: Images of *M. magnusii* at different magnifications, revealing the microscopic features of the colony structure when grown on CDS medium for seven days. (a) Zoomed view of a colony exhibiting the spiral morphology. (b) A spiral branch showing hyphae and conidia. (c) Full view of a *M. magnusii* colony after seven days of growth on YNB with high colony density. We use this colony when inferring parameters to compare the model and experiment.

3 Mathematical modelling and parameter inference methods

We aim to develop procedures for mathematical modelling and parameter inference that can apply to a variety of yeast colony morphologies. This section describes off-lattice agent-based modelling and a parameter inference method using sequential neural likelihood estimation. We illustrate these methods on a *M. magnusii* spiral colony. The biological insight gained includes quantification of the branching angle in spiral-forming colonies, and understanding of how model parameters, and hence cellular behaviour, differs across experimental conditions.

3.1 Off-lattice agent-based model

Li et al. [36] developed a two-dimensional off-lattice agent-based model for filamentous *S. cerevisiae* colonies, where the filaments consisted of pseudo-hyphal cells. We adapt this prior model to *M. magnusii* colonies, which are formed from hyphae. Each hypha consists of many individual cells, forming long and tubular structures much longer than an individual cell, but of similar width. Consequently, hyphae do not proliferate by cellular budding, but still grow and fragment as the colony consumes nutrients. To model growth by hyphal extension, we assume that the colony consists of many rod-like agents as per Figures 2 and 3, and we assume that each agent has the same size. All agents are ellipses with major axis length 22.5 µm and minor axis length 7.5 µm, giving an aspect ratio of 3 [21]. In practice, we represent these ellipses as dodecagons in 2D. These agents can be either regular hyphae, which can produce new segments at four sites located on their sides at angles of $\pm 7\pi/16$ radians from the distal poles of the mother hyphae, or filament-forming hyphae, which can only produce a new segment at one site located at the distal end. To capture the anticlockwise spiralling, hyphae in filaments extend at a prescribed acute angle θ_p, measured anticlockwise from the orientation of the major axis of the segment. This angle is known to be acute [21], but has not been previously quantified, and a key contribution of our work will be to infer a posterior distribution for this angle. The model features are summarised in Figure 4.

We simulate hyphal growth until the colony reaches a prescribed number of agents, n_{max}, chosen in advance such that the simulation ends when the

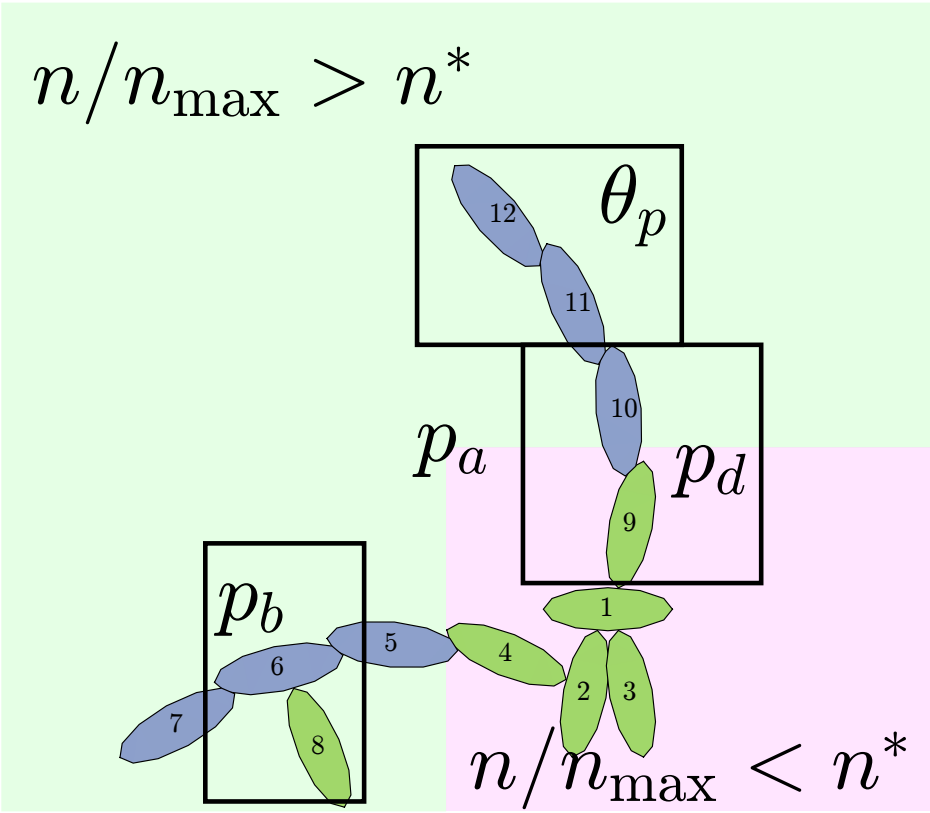

Figure 4: Cellular rules in the modified agent-based model. Regular hyphae that can extend from their sides are shown in green. Filament-forming hyphae that only extend at the angle θ_p from their distal ends are shown in dark blue. The numbers represent a possible sequence of hyphal growth, starting from hyphal segment 1, that could generate this pattern.

simulated colony has approximately the same area as an experimental colony. In our simulation, we begin hyphae reproduction by randomly selecting a hypha to produce a new segment. The behaviour of this hypha depends on five parameters, $\vec{\theta} = (n^*, p_a, p_b, p_d, \theta_p)$. On the length scale of *M. magnusii* experiments, nutrients are spatially uniform [64]. In the model, we use the existing colony area as a proxy for nutrient availability, such that hyphal filaments can emerge when the colony is sufficiently large. Consequently, we model neither time nor the nutrient concentration explicitly. The parameter

n^* is the threshold proportion of hyphae, relative to n_{max}, below which all hyphae can extend from both ends. When the number of cells in the simulated colony n exceeds the threshold, that is $n/n_{max} > n^*$, then filament-forming hyphae that extend from one end only can emerge.

Once $n/n_{max} > n^*$, the other probabilities p_a, p_b, and p_d determine the next hypha to extend, and the type of new agent that is produced. The probability p_a governs the type of hypha that extends. A regular hypha is selected with probability p_a, and a filament-forming hypha is selected with probability $1 - p_a$. The particular agent to extend is chosen at random from all agents of the relevant type. If a filament-forming hypha is selected, then the resulting agent will be a regular segment with probability p_b, or another filament-forming segment with probability $1 - p_b$. Conversely, if a regular hypha is selected to extend, then the resulting agent is filament-forming with probability p_d, or regular with probability $1 - p_d$. If the new agent is filament-forming, then the segment extends at the constant angle θ_p, measured anticlockwise from the orientation of the major axis of the original segment. We implement partial volume exclusion to prevent two agents from occupying the same space. If the centre of a proposed new agent would lie within the boundary of another agent, the event does not occur. The procedure then begins again from the start, and a new agent is selected to extend.

Since our agent-based modelling framework is similar to that applied to pseudohyphal growth [36], it is adaptable to other yeasts with different forms of growth. Should another yeast species that forms irregularly-shaped small colonies be studied, we could readily adapt this model, provided the agent size, budding patterns, and experimental colony area (in physical units) are known

or assumed in advance. In Li et al. [36], we have already applied the model to multiple strains of *S. cerevisiae* grown in different environments. The *M. magnusii* model presented here is one of many possible model variations, and demonstrates how the model can also apply to hyphal growth.

3.2 Image processing and summary statistics

We process experimental photographs and simulation results to quantify the spatial patterns. We convert experimental photographs to binary images using the Tool for Analysis of the Morphology of Microbial Colonies (TAMMiCol) [62], such that black pixels indicate regions occupied by the colony, and white pixels indicate unoccupied regions. The binary image for the *M. magnusii* colony is in Figure 5b. To enable direct comparison, we save images of the simulated colonies at the same scale and resolution as experimental photographs. We simulate colonies until they attain a target number of agents, which we prescribe. To obtain the target number of hyphae for the simulations that best fits the experimental data, we use the golden section search to minimise the difference in colony area between the simulated and experimental colonies.

For both experimental and simulation results, we define five spatial statistics to characterise morphology: maximum radius (R_{max}), mean radius (R_{mean}), filamentous area (I_{A_F}), branch count (I_B), and compactness (I_C). The two radii provide two measures of colony size. The maximum radius is the largest distance from the colony centroid to an occupied pixel, and the mean radius is the average distance between the centroid and all

pixels on the colony perimeter. The colony centroid is found using MATLAB's `regionprops()` function. Filamentous area is the number of occupied pixels between the mean and maximum radii, and therefore quantifies the extent of the hyphal branching pattern. Branch count quantifies the complexity of the hyphal filament pattern, and is the number of segments identified in a skeletonised image produced using MATLAB's `bwmorph()` function, that lie between the mean and maximum radii. Figure 5c provides an example of a skeletonised image. Compactness is the ratio between the colony perimeter and the perimeter of a circle with the same area as the colony, and quantifies the shape irregularity of the colony. Compactness is defined as $I_c = P/(4\pi A)$, where P is the number of occupied pixels on the colony perimeter (including holes within the colony), and A is the total number of occupied pixels in the colony. The perimeter is determined using MATLAB's `bwperim()` function. To weight each summary statistic equally, we ensure that each statistic only takes values on the unit interval by dividing each summary statistic by the maximum observed value of that statistic from 2000 simulations of the agent-based model.

3.3 Inference using sequential neural likelihood

Our model contains parameters governing an agent's behaviour that cannot be observed on the microscopic scale of a single agent. Therefore, we need to infer these parameters by comparing the macroscopic output of the model with experiments. Due to the high-dimensional output of our model, we do not have closed-form expressions for the likelihood function. So, we use likelihood-

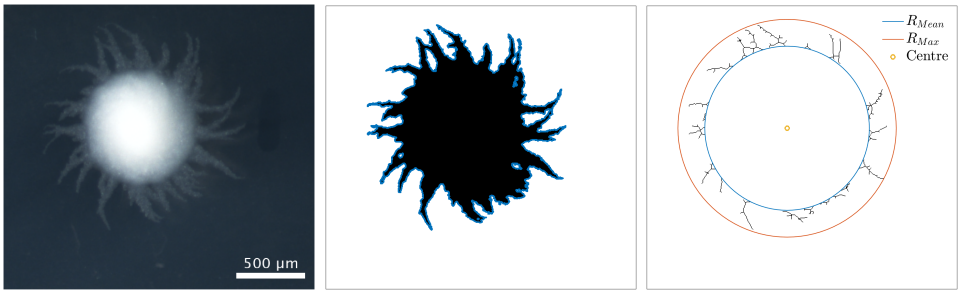

(a) (b) (c)

Figure 5: Visualisation of the summary statistics used in this paper. (a) Original experimental photograph of a *M. magnusii* colony with spiral hyphae. (b) Binary image with area overlayed with perimeter (blue). (c) Mean and maximum radii overlayed with the skeletonisation of the binary image in (b).

free Bayesian inference to compute approximate posterior distributions for the model parameters given an experimental photograph. Since yeast colonies contain approximately 30,000 agents that each may behave differently, and the model contains rules for volume exclusion, each simulation of the model takes on the order of five minutes to run. Previous approaches have used approximate Bayesian computation for inference [36], but the average run time of our model makes this prohibitively slow. Instead, we adopt a sequential neural likelihood (SNL) method [48, 3]. This method uses simulated data to train a conditional density estimator for the likelihood function. We can then sample from the posterior distribution using a standard Metropolis–Hastings Markov Chain Monte Carlo (MH-MCMC) approach [26], by substituting the approximate likelihood for the true function. The sequential naming of the algorithm refers to how the likelihood approximation is trained over a number of rounds, such that the majority of the data is from areas of high posterior density resulting in an accurate approximation [48]. We use a Gaussian mixture density network as our surrogate likelihood model [9],

which is implemented using the Julia package `MixtureDensityNetworks.jl`. More details on the training procedure are provided in Li et al. [35]. The main difference to this previous work is that we require a sequential method for this problem, whereas Li et al. [35] only used a single round of training.

4 Model simulation and parameter inference results

We perform the inference on a single experimental image to avoid issues of inter-experiment variability. We used uniform priors on the interval [0,1] for all parameters except for θ_p, which is uniform on the interval $[0,\pi/20]$. A pair plot of the resulting posterior distribution is shown in Figure 6. Figure 7 shows prior and posterior predictive distributions for the five summary statistics, and Figure 8 shows simulations from eight sets of parameters randomly sampled from the posterior. The observed summary statistics are in all cases in the tails of the prior predictive distribution, but the posterior predictive distributions' modes are mostly centred on them, indicating that the inference algorithm is performing correctly. Figure 8 provides an additional visual demonstration that the inferred parameters are capturing the correct morphology with hyphal branching patterns resembling the experimental image.

As expected, the threshold for initiation of spiral filamentation, n^*, is is inferred precisely with a small variance. This parameter is essential in controlling when filamentation begins. Another important parameter is p_d, which is inferred to be small. If p_d is small, we expect fewer longer spiralling

filaments, whereas a large p_d would produce more, shorter spiralling filaments. From the experimental images, we anticipate smaller values of p_d because filaments are distinct and long and this is confirmed by the posterior. Moreover, another crucial parameter in our model is the branching angle, θ_p, as this determines the amount of spiralling. This parameter could be identified, and its mode is around 0.04 radians (2.3 degrees). This result provides an estimate of the branching angle, which has not previously been quantified for *M. magnusii*. Although the branching angle is small, it still gives rise to observable colony-scale spiral patterns, as Figure 8 shows. The other parameters are either weakly informative or uninformative. The probability p_a governs whether a regular or filament-forming hypha is chosen to produce a new segment. This parameter is uninformative, suggesting that capturing the initial emergence of filament-forming hyphae and the branching angle are more important for predicting the morphological features captured by the summary statistics. Similarly, p_b is uninformative. Changes to this parameter influence the thickness of the filaments by allowing regular hyphae to form alongside filament-forming ones. Since our summary statistics do not contain a metric that explicitly quantifies the width of filaments, this parameter cannot be well inferred.

The statistics for maximum radius, mean radius, and compactness are especially well-predicted by our posterior predictive simulations (see Figure 7). There is larger variability in the filamentous area and branch count among the simulations, although overall the simulations still align well with the experiment. Variability in both the filamentous area and branch count is consistent with the finding that parameters affecting filament width are

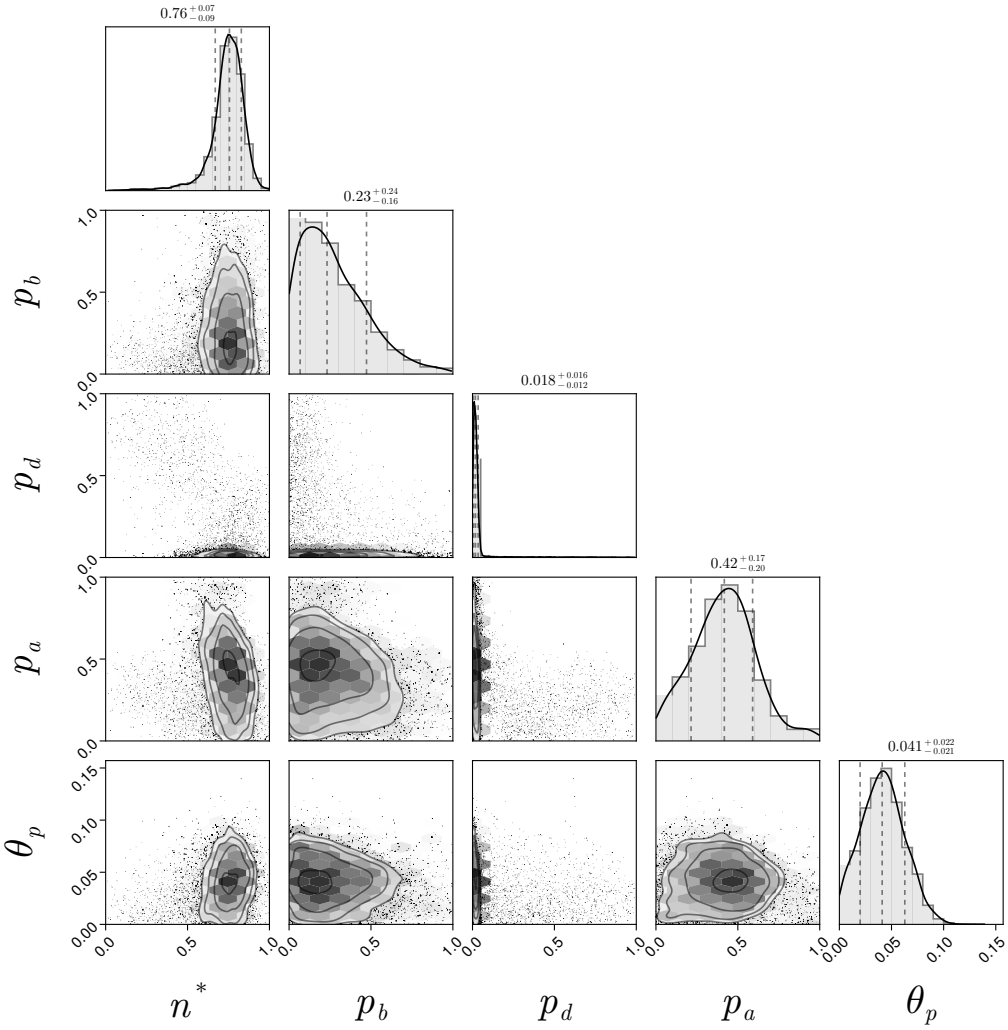

Figure 6: Pair plot of posterior distributions after three iterations of the sequential neural likelihood estimation.

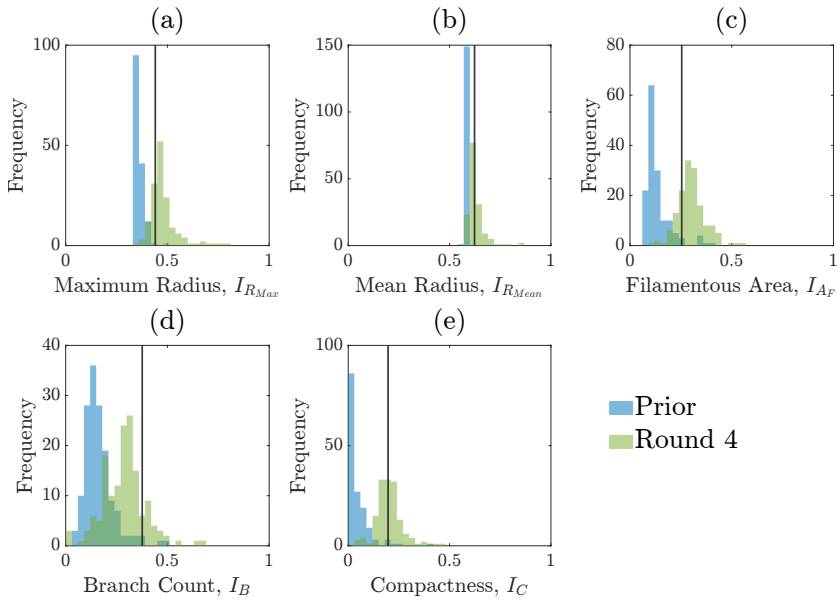

Figure 7: Normalised summary statistics generated from sampling from either the prior or from the posterior distribution after four rounds of SNLE. The vertical line represents the summary statistic from the experimental colony shown in Figure 5. Blue histograms are of the summary statistics for simulations sampled from the prior, and the green histograms are for simulations sampled from the posterior distribution after round 4 of the SNLE. (a) Maximum radius (b) Mean radius (c) Filamentous area (d) Branch count (e) Compactness.

uninformative due to the summary statistics not capturing filament width.

Overall, our procedure effectively captures colony size and circularity, but may not faithfully replicate the fine details in the hyphal branches.

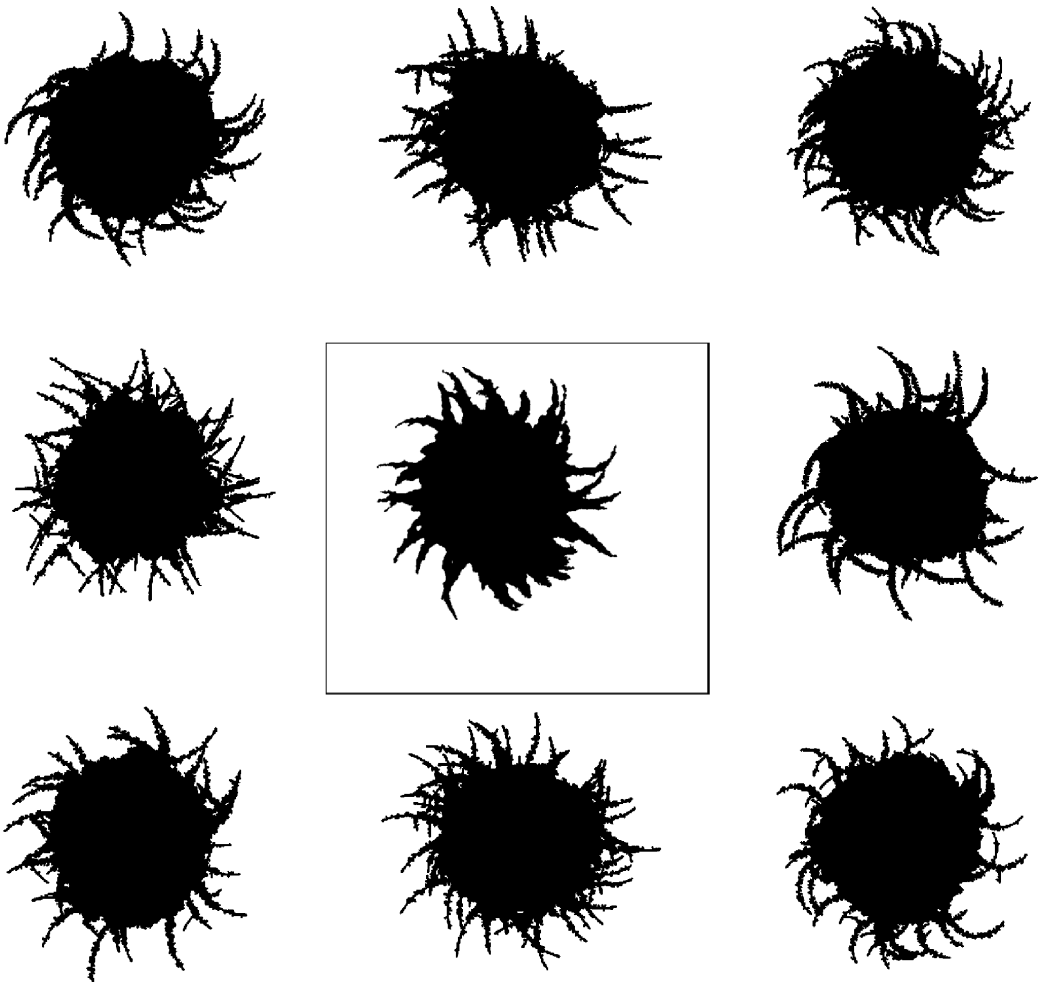

Figure 8: A binary image of an experimentally-produced colony of *M. magnusii* grown on YNB containing 150 mM ammonium sulfate (centre panel), flanked by eight simulations drawn from the posterior from Figure 6.

5 Other *M. magnusii* yeast morphologies

In different experimental conditions, *M. magnusii* colonies form different morphologies. We explore these morphologies through additional simulations of the model. In a nutrient-rich environment, the yeast tends to grow in a rounded hexagonal shape as shown in Figure 9a, reminiscent of Eden-like growth [23]. Although the round colony does not exhibit irregular filamentation, the almost hexagonal perimeter we see in the simulation mimics the experiment, which could be due to the shape and pattern of growth for regular hyphae. Under other conditions, *M. magnusii* has also been shown to have straight filaments of varying thicknesses as shown in Figures 9b and 9c. These patterns are more similar to the patterns formed by hyphal colonies of the important pathogenic yeast *C. albicans* [7, 18, 44]. With specifically-chosen parameter values, we can also capture these patterns in model simulations, as presented in Figures 9d–9f.

The ability to capture multiple experimentally-feasible *M. magnusii* morphologies suggests that our off-lattice model is consistent with the biology of hyphal growth. Furthermore, differences in parameter values across the three simulations in Figure 9 may indicate how the environment influences *M. magnusii* growth. In the hexagonal colony of Figures 9a and 9d, the threshold for filament-forming hyphae is set to $n^* = 1$, whereas this parameter is $n^* = 0.6$ and $n^* = 0.5$ for the other colonies. The experimental colony in Figure 9a was grown on CDS media with low density of colonies within the culture well, whereas the colonies in Figures 9b and 9c were grown under conditions of high colony density. The differences in n^* indicate that *M.*

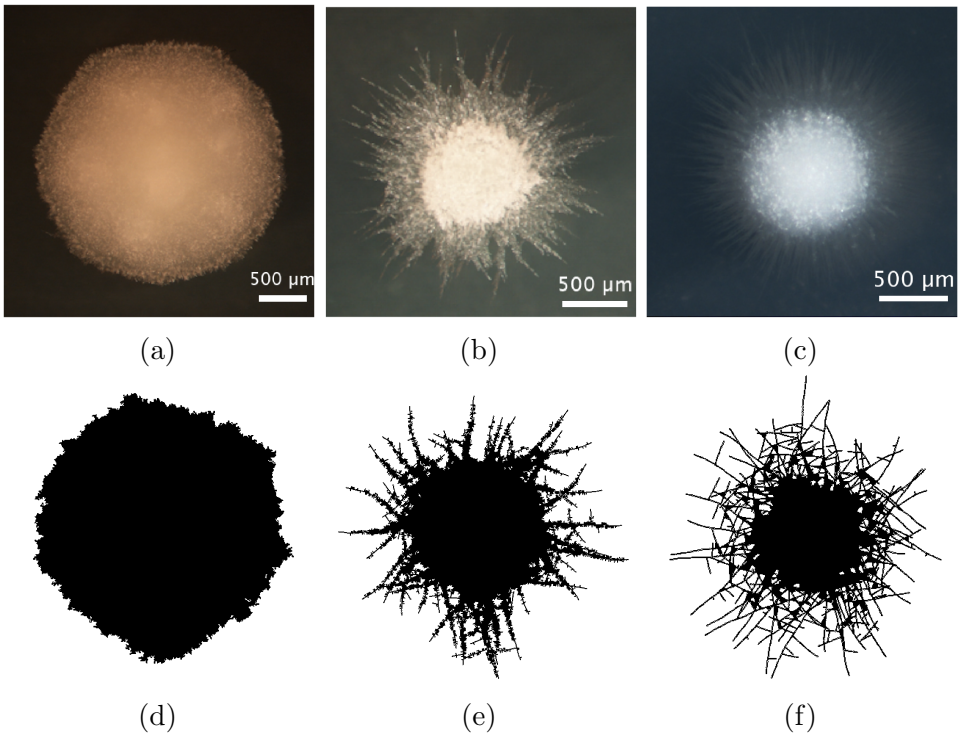

Figure 9: Other *M. magnusii* yeast morphologies under varying environmental conditions. (a) Experimental colony grown on CDS with low yeast density. (b) Experimental colony grown on CDS at high yeast density. (c) Experimental colony grown on YNB at high yeast density. (d) Simulation with $n_{\max} = 10,000$ agents and parameters $n^* = 1$, $p_a = 0.25$, $p_b = 0.3$, $p_d = 0.1$, and $\theta_p = 0.05$. (e) Simulation with $n_{\max} = 10,000$ agents and $n^* = 0.6$, $p_a = 0.25$, $p_b = 0.3$, $p_d = 0.1$, and $\theta_p = 0.05$. (f) Simulation with $n_{\max} = 10,000$ agents and $n^* = 0.5$, $p_a = 0.1$, $p_b = 0.02$, $p_d = 1$, and $\theta_p = 0.05$.

magnusii does not experience low-nutrient stress in the low colony density case, but does in high-density environments, where more colonies compete for the same nutrients. These results are consistent with the hypothesis that the transition between regular and filament-forming hyphae is mediated by nutrient availability. In contrast, the proliferation angle θ_p is held constant across all three simulations in Figures 9d–9f. Since θ_p was well-identified in parameter inference, this result suggests that the branching angle is con-

sistent, and could be an intrinsic feature of *M. magnusii* growth regardless of environment. Finally, although p_b was uninformative in the parameter estimation, comparing the simulations in Figures 9e and 9f reveals its impact. The simulation with larger p_b and smaller p_d favours thicker hyphal filaments (Figure 9e), because regular hyphal segments are more likely to occur within filaments. Conversely, the simulation with smaller p_b and larger p_d is more likely to produce filaments, but less likely to contain regular hyphae within filaments, creating the thinner filaments seen in Figure 9f.

6 Discussion and conclusion

In this paper, we have presented an off-lattice agent-based modelling and parameter inference procedure that yields biological insight into small yeast colonies formed in harsh environments. We applied this procedure to a new strain of *M. magnusii* recently bioprospected from a Tasmanian cider gum tree. Since this strain produced a spiral-like morphology, we adapted our agent-based model to incorporate hyphal segments and extension at a constant branching angle. We used image processing and spatial statistics to compare the shape of simulated colonies with the experiment. Using Bayesian inference, we estimated the mean of the branching angle as 2.3° [1.1°, 3.6°] (95% credible interval), a result that has not previously been quantified. The branching angle was one of the best-identified parameters, highlighting its importance to the spiral morphology. We showed that the colonies we simulated from our model using the inferred parameters closely resembled those from the experiment, and extended this result further to

obtain simulations of other experimentally-realised shapes with different parameters. We also provide open-source code for the agent-based models and parameter estimation techniques on GitHub.

Our work provides a framework for understanding the colony patterns formed by new yeast strains uncovered by bioprospecting. Adapting the agent-based model to meet the biological assumptions and performing parameter inference will allow researchers to gain insight into the key cell-level mechanisms underpinning the patterns. An improvement for future work would include a summary statistic to capture the thickness of branches, which might make the parameter p_b more informative. Additionally, this paper has reviewed several forms of surface growth in yeast colonies. However, in some experiments yeast cells grow on the surface and also penetrate into the agar medium [20]. This invasive growth is of great interest to biologists due to its importance for pathogenic infections. In future work, we intend to extend the modelling and parameter inference methods to three-dimensions to investigate this invasive growth phenomenon.

Acknowledgements KL acknowledges funding from the Australian Government through a Research Training Program (RTP) Scholarship. VJ, JEFG, BJB, and AKYT acknowledge funding from the Australian Research Council (Grant numbers DP230100406, and DE240100097). The authors acknowledge supercomputing resources from The University of Adelaide's maths1 High Performance Computing (HPC) service.

Code availability All code and data are available on GitHub at: `https://github.com/kaili2019/Li2025-Spiral-Yeast`.

References

[1] R. Abid et al. "Probiotic Yeast *Saccharomyces*: Back to Nature to Improve Human Health". In: *J. Fungi* 8.5 (2022), 444. ISSN: 2309-608X. DOI: 10.3390/jof8050444 (cit. on p. 3).

[2] S. Ahmad and W. Alfouzan. "*Candida auris*: Epidemiology, Diagnosis, Pathogenesis, Antifungal Susceptibility, and Infection Control Measures to Combat the Spread of Infections in Healthcare Facilities". In: *Microorganisms* 9.4 (2021), 807. DOI: 10.3390/microorganisms9040807 (cit. on p. 2).

[3] J. Alsing et al. "Fast Likelihood-Free Cosmology with Neural Density Estimators and Active Learning". In: *Mon. Not. R. Astron. Soc.* 488.3 (2019), pp. 4440–4458. ISSN: 0035-8711. DOI: 10.1093/mnras/stz1960 (cit. on pp. 7, 15).

[4] K. S. Andersen et al. "Genetic Basis for *Saccharomyces cerevisiae* Biofilm in Liquid Medium". In: *G3 (Bethesda)* 4.9 (2014), pp. 1671–1680. ISSN: 2160-1836. DOI: 10.1534/g3.114.010892. PMID: 25009170 (cit. on p. 3).

[5] M. Banwarth-Kuhn, J. Collignon, and S. Sindi. "Quantifying the Biophysical Impact of Budding Cell Division on the Spatial

Organization of Growing Yeast Colonies". In: *Appl. Sci.* 10.17 (2020), 5780. ISSN: 2076-3417. DOI: 10.3390/app10175780 (cit. on p. 6).

[6] A. Beauvais et al. "Characterization of a Biofilm-like Extracellular Matrix in FLO1-expressing *Saccharomyces cerevisiae* Cells". In: *FEMS Yeast Res.* 9.3 (2009), pp. 411–419. ISSN: 1567-1356. DOI: 10.1111/j.1567-1364.2009.00482.x (cit. on p. 3).

[7] J. Berman and P. E. Sudbery. "*Candida albicans*: A Molecular Revolution Built on Lessons from Budding Yeast". In: *Nat. Rev. Genet.* 3.12 (2002), pp. 918–931. ISSN: 1471-0064. DOI: 10.1038/nrg948 (cit. on pp. 3, 6, 21).

[8] B. J. Binder et al. "Quantifying Two-Dimensional Filamentous and Invasive Growth Spatial Patterns in Yeast Colonies". In: *PLoS Comput. Biol.* 11.2 (2015), e1004070. ISSN: 1553-7358. DOI: 10.1371/journal.pcbi.1004070 (cit. on pp. 2, 4, 5).

[9] C. M. Bishop. *Mixture Density Networks*. Technical Report. Birmingham: Aston University, 1994, pp. 1–25. URL: https://publications.aston.ac.uk/id/eprint/373/ (visited on 08/04/2025) (cit. on p. 15).

[10] R. K. Bojsen, K. S. Andersen, and B. Regenberg. "*Saccharomyces cerevisiae* — a Model to Uncover Molecular Mechanisms for Yeast Biofilm Biology". In: *FEMS Immunol. Med. Microbiol.* 65.2 (2012), pp. 169–182. ISSN: 0928-8244. DOI: 10.1111/j.1574-695X.2012.00943.x (cit. on p. 3).

[11] G. P. Boswell and F. A. Davidson. "Modelling Hyphal Networks". In: *Fungal Biol. Rev.* 26.1 (2012), pp. 30–38. DOI: 10.1016/j.fbr.2012.02.002 (cit. on p. 2).

[12] D. Botstein, S. A. Chervitz, and M. Cherry. "Yeast as a Model Organism". In: *Science* 277.5330 (1997), pp. 1259–1260. DOI: 10.1126/science.277.5330.1259 (cit. on p. 3).

[13] P. J. Brown et al. "A Rigid Body Framework for Multicellular Modeling". In: *Nat. Comput. Sci.* 1.11 (2021), pp. 754–766. ISSN: 2662-8457. DOI: 10.1038/s43588-021-00154-4 (cit. on p. 7).

[14] A. P. Browning et al. "Inferring Parameters for a Lattice-Free Model of Cell Migration and Proliferation Using Experimental Data". In: *J. Theor. Biol.* 437 (2018), pp. 251–260. ISSN: 0022-5193. DOI: 10.1016/j.jtbi.2017.10.032 (cit. on p. 7).

[15] M. Čáp et al. "Cell Differentiation within a Yeast Colony: Metabolic and Regulatory Parallels with a Tumor-Affected Organism". In: *Mol. Cell* 46.4 (2012), pp. 436–448. ISSN: 1097-2765. DOI: 10.1016/j.molcel.2012.04.001. PMID: 22560924 (cit. on p. 3).

[16] D. Carmona-Gutierrez et al. "Guidelines and Recommendations on Yeast Cell Death Nomenclature". In: *Microb. Cell* 5.1 (2018), pp. 4–31. ISSN: 2311-2638. DOI: 10.15698/mic2018.01.607. PMID: 29354647 (cit. on p. 3).

[17] L. Chen et al. "Two-Dimensonality of Yeast Colony Expansion Accompanied by Pattern Formation". In: *PLoS Comput. Biol.* 10.12 (2014), e1003979. DOI: 10.1371/journal.pcbi.1003979 (cit. on p. 6).

[18] I. A. Cleary et al. "Pseudohyphal Regulation by the Transcription Factor Rfg1p in *Candida albicans*". In: *Eukaryot. Cell* 9.9 (2010), pp. 1363–1373. DOI: 10.1128/ec.00088-10 (cit. on pp. 6, 21).

[19] P. J. Cullen and G. F. Sprague. "Glucose Depletion Causes Haploid Invasive Growth in Yeast". In: *Proc. Natl. Acad. Sci. U.S.A.* 97.25 (2000), pp. 13619–13624. DOI: 10.1073/pnas.240345197 (cit. on p. 2).

[20] Paul J. Cullen and George F. Sprague. "Glucose depletion causes haploid invasive growth in yeast". In: *Proceedings of the National Academy of Sciences* 97 (2000), pp. 13619–13624 (cit. on p. 24).

[21] G. S. de Hoog and M. T. Smith. "*Magnusiomyces* Zender (1977)". In: *The Yeasts (Fifth Edition)*. Ed. by C. P. Kurtzman, J. W. Fell, and T. Boekhout. London: Elsevier, 2011, pp. 565–574. ISBN: 978-0-444-52149-1. DOI: 10.1016/B978-0-444-52149-1.00045-8 (cit. on pp. 6, 10).

[22] J. Dyer et al. "Black-Box Bayesian Inference for Agent-Based Models". In: *J. Econ. Dyn. Control* 161 (2024), 104827. ISSN: 0165-1889. DOI: 10.1016/j.jedc.2024.104827 (cit. on p. 7).

[23] M. Eden. "A Two-Dimensional Growth Process". In: *Proceedings of the Fourth Berkeley Symposium on Mathematical Statistics and Probability, Volume 4: Contributions to Biology and Problems of Medicine*. Vol. 4.4. University of California Press, 1961, pp. 223–240 (cit. on pp. 6, 21).

[24] A. J. Gallo et al. "Modelling Uniaxial Non-Uniform Yeast Colony Growth: Comparing an Agent-Based Model and Continuum

Approximations". In: *J. Theor. Biol.* 523 (2021), 110715. ISSN: 0022-5193. DOI: 10.1016/j.jtbi.2021.110715 (cit. on p. 7).

[25] J. M. Gardner et al. "Modern Yeast Development: Finding the Balance between Tradition and Innovation in Contemporary Winemaking". In: *FEMS Yeast Res.* 23 (2023), foac049. ISSN: 1567-1356. DOI: 10.1093/femsyr/foac049 (cit. on p. 3).

[26] Charles J Geyer. "Practical markov chain monte carlo". In: *Statistical science* (1992), pp. 473–483 (cit. on p. 15).

[27] C. J. Gimeno et al. "Unipolar Cell Divisions in the Yeast *S. cerevisiae* Lead to Filamentous Growth: Regulation by Starvation and RAS". In: *Cell* 68.6 (1992), pp. 1077–1090. ISSN: 0092-8674. DOI: 10.1016/0092-8674(92)90079-R (cit. on pp. 2, 3, 5).

[28] A. Goffeau et al. "Life with 6000 Genes". In: *Science* 274.5287 (1996), pp. 546–567. DOI: 10.1126/science.274.5287.546 (cit. on p. 2).

[29] C. W. Gourlay, W. Du, and K. R. Ayscough. "Apoptosis in Yeast – Mechanisms and Benefits to a Unicellular Organism". In: *Mol. Microbiol.* 62.6 (2006), pp. 1515–1521. ISSN: 1365-2958. DOI: 10.1111/j.1365-2958.2006.05486.x (cit. on p. 3).

[30] D. A. Hogan, Å. Vik, and R. Kolter. "A *Pseudomonas aeruginosa* Quorum-Sensing Molecule Influences *Candida albicans* Morphology". In: *Mol. Microbiol.* 54.5 (2004), pp. 1212–1223. ISSN: 1365-2958. DOI: 10.1111/j.1365-2958.2004.04349.x (cit. on p. 3).

[31] V. Jiranek. "The Prospect of Superior Yeast for Winemaking: Recent Successes through Bioprospecting". In: *Curr. Opin. Biotechnol.* 90 (2024), 103200. ISSN: 0958-1669. DOI: 10.1016/j.copbio.2024.103200 (cit. on p. 3).

[32] J. J. Klowss et al. "A Stochastic Mathematical Model of 4D Tumour Spheroids with Real-Time Fluorescent Cell Cycle Labelling". In: *J. R. Soc. Interface* 19.189 (2022), 20210903. DOI: 10.1098/rsif.2021.0903 (cit. on p. 7).

[33] E. M. Kojic and R. O. Darouiche. "*Candida* Infections of Medical Devices". In: *Clin. Microbiol. Rev.* 17.2 (2004), pp. 255–267. DOI: 10.1128/cmr.17.2.255-267.2004 (cit. on p. 2).

[34] K. Li et al. "A Mathematical Model for Nutrient-Limited Uniaxial Growth of a Compressible Tissue". In: *J. Theor. Biol.* 575 (2023), 111631. ISSN: 0022-5193. DOI: 10.1016/j.jtbi.2023.111631 (cit. on p. 6).

[35] K. Li et al. *Agent-Based Modelling and Time Series Inference of Filamentous Yeast Colonies*. 2025. Pre-published (cit. on p. 16).

[36] K. Li et al. "An Off-Lattice Discrete Model to Characterise Filamentous Yeast Colony Morphology". In: *PLoS Comput. Biol.* 20.11 (2024), e1012605. DOI: 10.1371/journal.pcbi.1012605 (cit. on pp. 2, 6, 10, 12, 13, 15).

[37] K. Li et al. *Multiscale Analysis of* Candida albicans *Biofilms*. 2025. Pre-published (cit. on p. 4).

[38] Z. Liu, J. Wang, and J. Nielsen. "Yeast Synthetic Biology Advances Biofuel Production". In: *Curr. Opin. Microbiol.* 65 (2022), pp. 33–39. ISSN: 1369-5274. DOI: 10.1016/j.mib.2021.10.010 (cit. on p. 3).

[39] L. M. Martinez and B. C. Fries. "Fungal Biofilms: Relevance in the Setting of Human Disease". In: *Curr. Fungal Infect. Rep.* 4.4 (2010), pp. 266–275. DOI: 10.1007/s12281-010-0035-5 (cit. on p. 2).

[40] A. Meškauskas, M. D. Fricker, and D. Moore. "Simulating Colonial Growth of Fungi with the Neighbour-Sensing Model of Hyphal Growth". In: *Mycol. Res.* 108.11 (2004), pp. 1241–1256. ISSN: 09537562. DOI: 10.1017/S0953756204001261 (cit. on p. 2).

[41] A. Meškauskas, L. J. McNulty, and D. Moore. "Concerted Regulation of All Hyphal Tips Generates Fungal Fruit Body Structures: Experiments with Computer Visualizations Produced by a New Mathematical Model of Hyphal Growth". In: *Mycol. Res.* 108.4 (2004), pp. 341–353. ISSN: 09537562. DOI: 10.1017/S0953756204009670 (cit. on p. 2).

[42] W. J. Middelhoven, B. Broekhuizen, and J. van Eijk. "Detection, with the Dye Phloxine B, of Yeast Mutants Unable to Utilize Nitrogenous Substances as the Sole Nitrogen Source". In: *J. Bacteriol.* 128.3 (1976), pp. 851–852. DOI: 10.1128/jb.128.3.851-852.1976 (cit. on p. 5).

[43] N. Minois et al. "Advances in Measuring Lifespan in the Yeast *Saccharomyces cerevisiae*". In: *Proc. Natl. Acad. Sci. U.S.A.* 102.2 (2005), pp. 402–406. DOI: 10.1073/pnas.0408332102 (cit. on p. 3).

[44] S. Mohammadi et al. "Amino Acid Substitutions in Specific Proteins Correlate with Farnesol Unresponsiveness in *Candida albicans*". In: *BMC Genom.* 24.1 (2023), 93. ISSN: 1471-2164. DOI: 10.1186/s12864-023-09174-y (cit. on pp. 6, 21).

[45] D. J. Netherwood et al. "Accidental and Regulated Cell Death in Yeast Colony Biofilms". In: *Bull. Math. Biol.* 87 (2025), 110. DOI: 10.1101/2025.02.02.636168 (cit. on pp. 4, 5).

[46] K. W. Nickerson, A. L. Atkin, and J. M. Hornby. "Quorum Sensing in Dimorphic Fungi: Farnesol and Beyond". In: *Appl. Environ. Microbiol.* 72.6 (2006), pp. 3805–3813. DOI: 10.1128/AEM.02765-05 (cit. on p. 3).

[47] Z. Palková and L. Váchová. "Cell Differentiation, Aging, and Death in Spatially Organized Yeast Communities: Mechanisms and Consequences". In: *Cell Death Differ.* (2025), pp. 1–13. ISSN: 1476-5403. DOI: 10.1038/s41418-025-01485-9 (cit. on p. 3).

[48] G. Papamakarios, D. Sterratt, and I. Murray. "Sequential Neural Likelihood: Fast Likelihood-Free Inference with Autoregressive Flows". In: *Proceedings of the Twenty-Second International Conference on Artificial Intelligence and Statistics*. The 22nd International Conference on Artificial Intelligence and Statistics. Proceedings of Machine Learning Research, 2019, pp. 837–848. URL: https://proceedings.mlr.press/v89/papamakarios19a.html (visited on 08/04/2025) (cit. on pp. 7, 15).

[49] D. R. Pentland et al. "CO_2 Enhances the Formation, Nutrient Scavenging and Drug Resistance Properties of *C. albicans* Biofilms".

In: *npj Biofilms Microbiomes* 7.1 (1 2021), 67. ISSN: 2055-5008. DOI: 10.1038/s41522-021-00238-z (cit. on p. 5).

[50] M. A. Pfaller et al. "Epidemiology and Outcomes of Invasive Candidiasis Due to Non-Albicans Species of *Candida* in 2,496 Patients: Data from the Prospective Antifungal Therapy (PATH) Registry 2004–2008". In: *PLoS One* 9.7 (2014), e101510. ISSN: 1932-6203. DOI: 10.1371/journal.pone.0101510 (cit. on p. 2).

[51] A. Pietz, K. John, and U. Thiele. "The Role of Substrate Mechanics in Osmotic Biofilm Spreading". In: *Soft Matter* 21.15 (2025), pp. 2935–2945. ISSN: 1744-6848. DOI: 10.1039/D4SM01463D (cit. on p. 3).

[52] V. Plocek et al. "Cell Distribution within Yeast Colonies and Colony Biofilms: How Structure Develops". In: *Int. J. Mol. Sci.* 21 (2020), 3873. DOI: 10.3390/ijms21113873 (cit. on p. 3).

[53] A. R. Pokhrel et al. *Cell-Substrate Friction Controls Biofilm Development*. 2025. DOI: 10.1101/2025.07.11.664457. Pre-published (cit. on p. 3).

[54] T. B. Reynolds and G. R. Fink. "Bakers' Yeast, a Model for Fungal Biofilm Formation". In: *Science* 291.5505 (2001), pp. 878–881. DOI: 10.1126/science.291.5505.878 (cit. on pp. 3, 4).

[55] T. B. Reynolds et al. "Mat Formation in *Saccharomyces cerevisiae* Requires Nutrient and pH Gradients". In: *Eukaryotic Cell* 7.1 (2008), pp. 122–130. DOI: 10.1128/ec.00310-06 (cit. on pp. 3, 4).

[56] S. Schelenz et al. "First Hospital Outbreak of the Globally Emerging *Candida auris* in a European Hospital". In: *Antimicrob. Resist. Infect. Control* 5.1 (2016), 35. ISSN: 2047-2994. DOI: 10.1186/s13756-016-0132-5 (cit. on p. 2).

[57] A. Tam et al. "A Thin-Film Extensional Flow Model for Biofilm Expansion by Sliding Motility". In: *Proc. Royal Soc. A* 475.2229 (2019), 20190175. DOI: 10.1098/rspa.2019.0175 (cit. on p. 6).

[58] A. Tam et al. "Nutrient-Limited Growth with Non-Linear Cell Diffusion as a Mechanism for Floral Pattern Formation in Yeast Biofilms". In: *J. Theor. Biol.* 448 (2018), pp. 122–141. DOI: 10.1016/j.jtbi.2018.04.004 (cit. on pp. 3–6).

[59] A. K. Y. Tam et al. *Quantifying the Effects of Cell Death and Agar Density Using an Extensional Flow Model for Yeast Colony Biofilms.* 2025. Pre-published (cit. on p. 4).

[60] A. K. Y. Tam et al. "Thin-Film Lubrication Model for Biofilm Expansion under Strong Adhesion". In: *Phys. Rev. E* 105.1 (2022), 014408. DOI: 10.1103/PhysRevE.105.014408 (cit. on p. 6).

[61] E. L. Tek et al. "Evaluation of the Ability of Commercial Wine Yeasts to Form Biofilms (Mats) and Adhere to Plastic: Implications for the Microbiota of the Winery Environment". In: *FEMS Microbiol. Ecol.* 94.2 (2018), fix188. DOI: 10.1093/femsec/fix188 (cit. on p. 3).

[62] H. Tronnolone et al. "Diffusion-Limited Growth of Microbial Colonies". In: *Sci. Rep.* 8 (2018), 5992. DOI: 10.1038/s41598-018-23649-z (cit. on p. 13).

[63] H. Tronnolone et al. "Quantifying the Dominant Growth Mechanisms of Dimorphic Yeast Using a Lattice-Based Model". In: *J. R. Soc. Interface* 14.134 (2017), 20170314. DOI: 10.1098/rsif.2017.0314 (cit. on pp. 4–6).

[64] H. Tronnolone et al. "TAMMiCol: Tool for Analysis of the Morphology of Microbial Colonies". In: *PLoS Comput. Biol.* 14.12 (2018), e1006629. ISSN: 1553-7358. DOI: 10.1371/journal.pcbi.1006629 (cit. on pp. 3, 5, 11).

[65] L. Váchová and Z. Palková. "Physiological Regulation of Yeast Cell Death in Multicellular Colonies Is Triggered by Ammonia". In: *J. Cell Biol.* 169.5 (2005), pp. 711–717. ISSN: 0021-9525. DOI: 10.1083/jcb.200410064 (cit. on p. 3).

[66] L. Váchová et al. "Flo11p, Drug Efflux Pumps, and the Extracellular Matrix Cooperate to Form Biofilm Yeast Colonies". In: *J. Cell Biol.* 194.5 (2011), pp. 679–687. ISSN: 0021-9525. DOI: 10.1083/jcb.201103129 (cit. on p. 3).

[67] C. Vulin et al. "Growing Yeast into Cylindrical Colonies". In: *Biophys. J.* 106.10 (2014), pp. 2214–2221. ISSN: 0006-3495. DOI: 10.1016/j.bpj.2014.02.040 (cit. on pp. 3, 5).

[68] X. Wang et al. "Calibration of Agent Based Models for Monophasic and Biphasic Tumour Growth Using Approximate Bayesian Computation". In: *J. Math. Biol.* 88.3 (2024), 28. ISSN: 1432-1416. DOI: 10.1007/s00285-024-02045-4 (cit. on p. 7).

[69] R. G. Willaert. "Adhesins of Yeasts: Protein Structure and Interactions". In: *J. Fungi (Basel)* 4.4 (2018), 119. ISSN: 2309-608X. DOI: 10.3390/jof4040119. PMID: 30373267 (cit. on p. 3).

A Multiple agent sizes

We also investigate the impact of agent shape on the spiral yeast morphology. To demonstrate the colony morphology is robust to changes in agent shape, we simulate colonies where the regular hyphal segments and branching hyphal segments have different geometry. We use the same parameter values as in Figure 8, varying only the agent shape. There is minimal difference between the three colonies, suggesting that other parameters such as the branching angle drive the spiral colony morphology in *M. magnusii*.

(a) (b) (c)

Figure 10: (a) Experiment of *M. magnusii* grown on YNB medium. (b) Spiral yeast simulation with parameters $n^* = 0.76$, $p_a = 0.42$, $p_b = 0.23$, $p_d = 0.02$, and $\theta_p = 0.04$, drawn from the posterior distribution. All agents have the same size, with aspect ratio 0.33. (c) Spiral yeast simulation with parameters $n^* = 0.76$, $p_a = 0.42$, $p_b = 0.23$, $p_d = 0.02$, and $\theta_p = 0.04$, drawn from the posterior distribution. There are two possible agent sizes, with aspect ratios 0.75 and 0.33. Each agent has the same area.

B Parameter inference results

The following figures summarise the summary statistics obtained after each round of sequential neural likelihood applied to the experimental image.

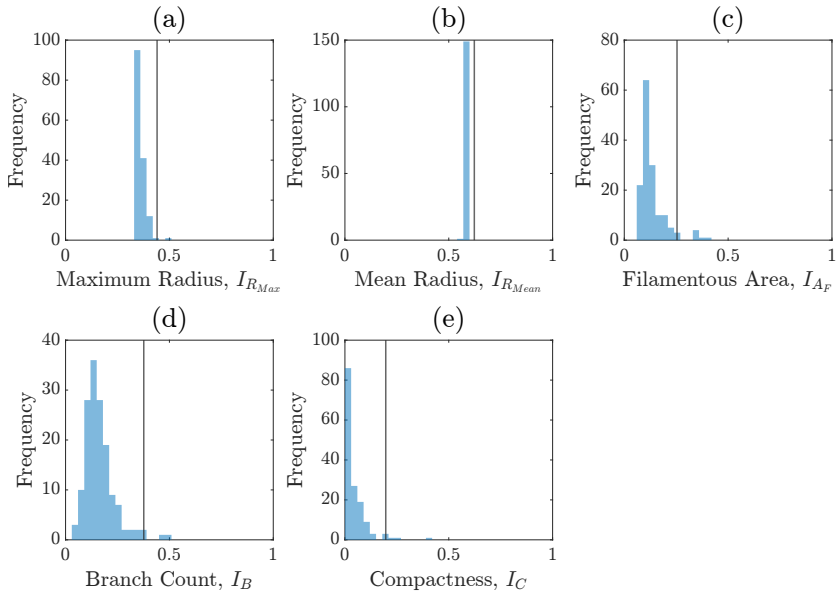

Figure 11: Summary statistics of the priors.

Author addresses

1. **Kai Li**, School of Computer and Mathematical Sciences, University of Adelaide, Adelaide SA 5005, Australia.

2. **Andrew J. Black**, School of Computer and Mathematical Sciences, University of Adelaide, Adelaide SA 5005, Australia.

3. **Tea Knežević**, Discipline of Wine Science, Waite Campus, University of Adelaide, Urrbrae SA 5064, Australia.

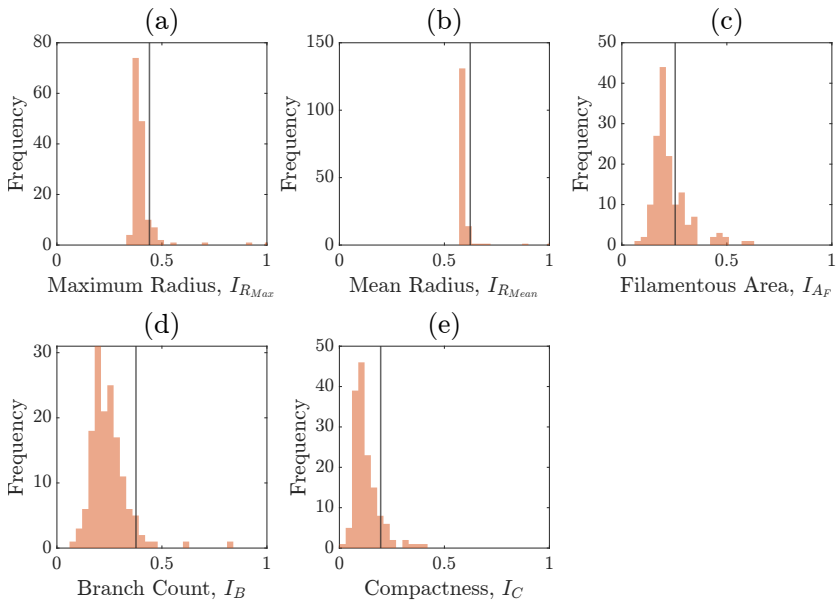

Figure 12: Summary statistics of round one.

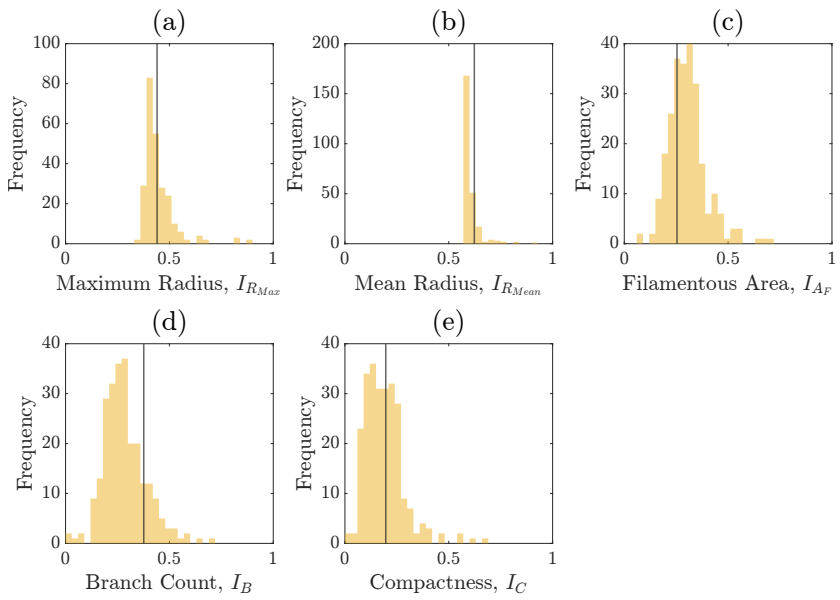

Figure 13: Summary statistics of round two.

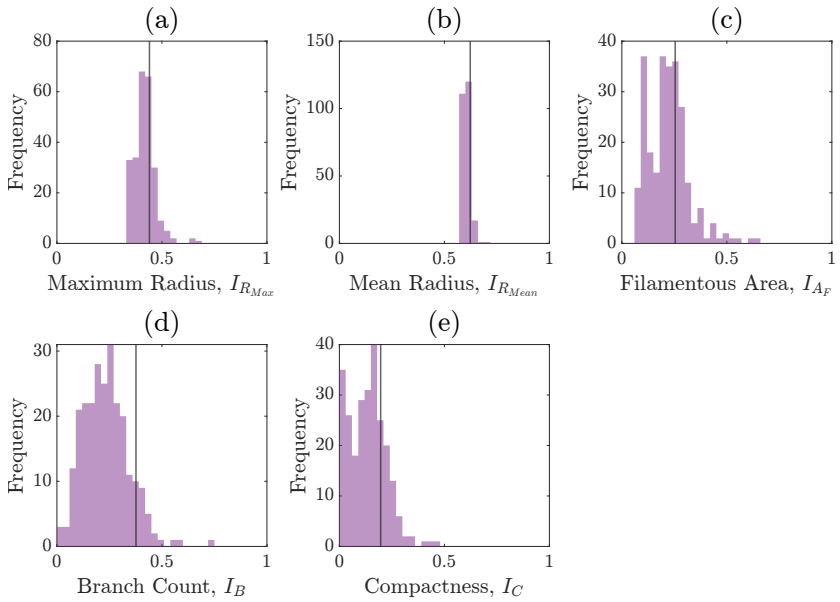

Figure 14: Summary statistics of round three.

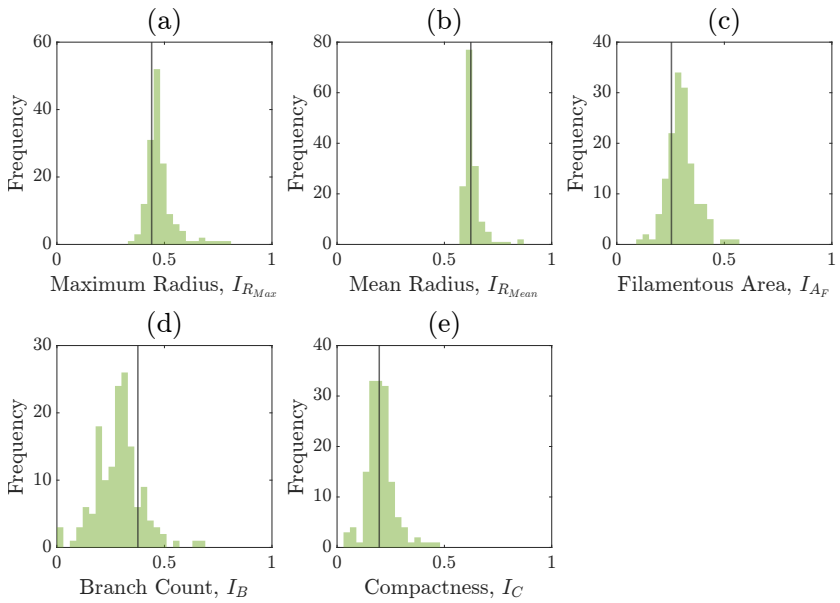

Figure 15: Summary statistics of round four.

4. **Jennifer M. Gardner**, Discipline of Wine Science, Waite Campus, University of Adelaide, Urrbrae SA 5064, Australia.

5. **Jin Zhang**, Discipline of Wine Science, Waite Campus, University of Adelaide, Urrbrae SA 5064, Australia.

6. **Vladimir Jiranek**, School of Biological Sciences, The University of Southampton, Southampton SO17 1BJ, United Kingdom.
Discipline of Wine Science, Waite Campus, University of Adelaide, Urrbrae SA 5064, Australia.

7. **J. Edward F. Green**, School of Computer and Mathematical Sciences, University of Adelaide, Adelaide SA 5005, Australia.

8. **Benjamin J. Binder**, School of Computer and Mathematical Sciences, University of Adelaide, Adelaide SA 5005, Australia.

9. **Alexander K. Y. Tam**, UniSA STEM, The University of South Australia, Mawson Lakes SA 5095, Australia.
`mailto:alex.tam@unisa.edu.au`
`orcid:0000-0003-3565-1068`